The crystal structure of human protein farnesyltransferase reveals the basis for inhibition by CaaX tetrapeptides and their mimetics

Stephen B. Long*, Paula J. Hancock†, Astrid M. Kral†, Homme W. Hellinga*, and Lorena S. Beese*‡

*Department of Biochemistry, Duke University Medical Center, Durham, NC 27710; and †Department of Cancer Research, Merck Research Laboratories, West Point, PA 19486

Edited by Michael S. Brown, University of Texas Southwestern Medical Center, Dallas, TX, and approved September 21, 2001 (received for review August 2, 2001)

Protein farnesyltransferase (FTase) catalyzes the attachment of a farnesyl lipid group to the cysteine residue located in the C-terminal tetrapeptide of many essential signal transduction proteins, including members of the Ras superfamily. Farnesylation is essential both for normal functioning of these proteins, and for the transforming activity of oncogenic mutants. Consequently FTase is an important target for anti-cancer therapeutics. Several FTase inhibitors are currently undergoing clinical trials for cancer treatment. Here, we present the crystal structure of human FTase, as well as ternary complexes with the TKCVFM hexapeptide substrate, CVFM non-substrate tetrapeptide, and L-739,750 peptidomimetic with either farnesyl diphosphate (FPP), or a nonreactive analogue. These structures reveal the structural mechanism of FTase inhibition. Some CaaX tetrapeptide inhibitors are not farnesylated, and are more effective inhibitors than farnesylated CaaX tetrapeptides. CVFM and L-739,750 are not farnesylated, because these inhibitors bind in a conformation that is distinct from the TKCVFM hexapeptide substrate. This non-substrate binding mode is stabilized by an ion pair between the peptide N terminus and the α-phosphate of the FPP substrate. Conformational mapping calculations reveal the basis for the sequence specificity in the third position of the CaaX motif that determines whether a tetrapeptide is a substrate or non-substrate. The presence of β-branched amino acids in this position prevents formation of the non-substrate conformation; all other aliphatic amino acids in this position are predicted to form the non-substrate conformation, provided their N terminus is available to bind to the FPP α-phosphate. These results may facilitate further development of FTase inhibitors.

Many intracellular proteins are posttranslationally modified by the attachment of lipids (1). Protein farnesyltransferase (FTase), geranylgeranyltransferase type-I (GGTase-I), and geranylgeranyltransferase type-II (Rab geranylgeranyltransferase, GGTase-II) constitute the protein prenyltransferase family of lipid modifying enzymes (reviewed in ref. 2). These enzymes catalyze the formation of thioether linkages between the C1 atom of farnesyl (15-carbon by FTase) or geranylgeranyl (20-carbon by GGTase-I and -II) isoprenoid lipids and cysteine residues at or near the C terminus of protein acceptors. Protein substrates of the prenyltransferases include Ras, Rho, Rab, other Ras-related small GTP-binding proteins, γ subunits of heterotrimeric G-proteins, nuclear lamins, centromeric proteins, and many proteins involved in visual signal transduction (2, 3). The attached lipid is required for proper functioning of the modified protein by mediating membrane associations and specific protein–protein interactions. FTase and GGTase-I, which are collectively known as the CaaX prenyltransferases, attach their respective isoprenoid to the cysteine residue of a C-terminal CaaX motif (C, cysteine; a, typically an aliphatic residue; X, C-terminal residue). GGTase-II attaches geranylgeranyl groups to two C-terminal cysteine residues in the Rab family of Ras-related GTPases.

Ras must be associated with the plasma membrane for proper functioning in the signal transduction pathway. Prenylation of Ras is required for this subcellular localization and is essential for the transforming activity of oncogenic variants of Ras (4–6). FTase is therefore a potential target for anticancer therapeutics. A critical advance in the development of FTase inhibitors was the finding that tetrapeptides that conformed to the CaaX sequence motif are competitive inhibitors (7). Surprisingly, a subset of these tetrapeptides (e.g., CVFM) are not farnesylated (8). Two features were identified as dominant determinants for the lack of farnesylation: a positively charged N terminus and an aromatic residue at the a_2 position (9). The distinction between competitive inhibitors that are competent substrates and non-substrate inhibitors is an important one, because farnesylation of the competitive inhibitor decreases their affinity for the enzyme, thereby reducing potency (10). These findings led to the design of several peptidomimetic compounds based on the CaaX motif (reviewed in ref. 11). The initial hurdles of low cell permeability and susceptibility to proteolytic degradation inherent to peptide-based compounds were overcome by the synthesis of ester prodrugs, such as L-744,832 (Fig. 1), which inhibited the growth of more than 70% of tumor cell lines (12) and caused tumor regression in H-*ras* transformed mice, without systemic toxicity (13). Numerous inhibitors of FTase are now in clinical trials for the treatment of human cancer (reviewed in ref. 14). L-744,832 is the isopropyl ester prodrug of L-739,750 (Fig. 1; ref. 15), the peptidomimetic compound used in the structures presented in this paper, and was the first inhibitor of FTase to demonstrate tumor regression in animals (13).

The three-dimensional structures of FTase-bound peptidomimetics were initially characterized by NMR spectroscopy. Two-dimensional transferred nuclear Overhauser effect (TRNOE) experiments indicated that the peptide backbones of a CIFM peptide-based compound and the peptide CVWM adopt conformations similar to a β-turn when bound to FTase (16). This

This paper was submitted directly (Track II) to the PNAS office.

Abbreviations: FTase, protein farnesyltransferase; GGTase-I, protein geranylgeranyltransferase type-I; GGTase-II protein geranylgeranyltransferase type-II; FPP, farnesyl diphosphate.

Data deposition: The atomic coordinates and structure factors have been deposited in the Protein Data Bank, www.rcsb.org (PDB ID codes 1JCQ, 1JCR, and 1JCS corresponding to complexes of human FTase with FPP and L-739,750, rat FTase with FPP and the peptide CVFM, and rat FTase with an analog of FPP and the peptide TKCVFM, respectively).

‡To whom correspondence should be addressed at: Department of Biochemistry, Box 3711, Duke University Medical Center, Durham, NC 27710. E-mail: lsb@biochem.duke.edu.

The publication costs of this article were defrayed in part by page charge payment. This article must therefore be hereby marked "*advertisement*" in accordance with 18 U.S.C. §1734 solely to indicate this fact.

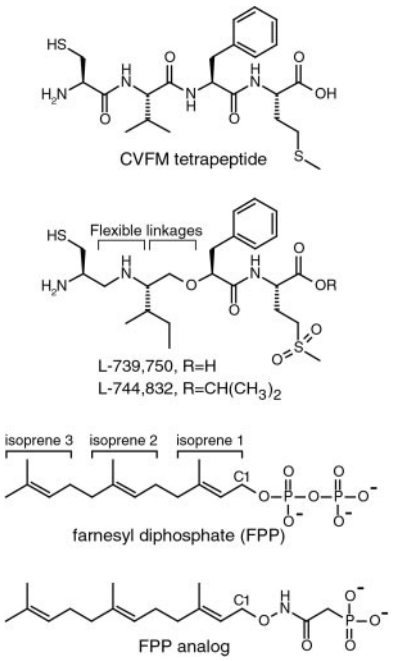

Fig. 1. Chemical structures.

information was used to design conformationally constrained peptidomimetic compounds that are very potent inhibitors of FTase (11). It was therefore surprising to find that, in crystal structures of FTase complexed with peptide substrates and farnesyl diphosphate analogs, the CaaX motifs adopted an extended conformation (17, 18) rather than a β-turn. In the crystal structures, the cysteine thiolate of the CaaX motif coordinates the catalytic zinc ion, consistent with UV-visible spectroscopic solution studies (19, 20). However, removal of the zinc ion converts the extended conformation to a β-turn in the crystal structure (18). This result suggests that the β-turn conformation observed by NMR studies represents a state in which the cysteine is not coordinated to the zinc ion.

Here, we present three crystal structures of FTase complexes (which include the first structure of human FTase) that provide a molecular basis for the mode of action of CaaX tetrapeptide inhibitors and their mimetics. We find that tetrapeptides adopt an extended conformation, rather than a β-turn, and we suggest a basis for the distinction between substrate and non-substrate inhibition.

Materials and Methods

Sample Preparation. To obtain heterodimeric human FTase in *Escherichia coli*, the two subunits were expressed as a translationally coupled operon under transcriptional control by the bacteriophage T7 promoter in the plasmid pT5T (21). Translational coupling was achieved by placing the α subunit coding sequence upstream of the β subunit coding sequence. A microtubule epitope, Glu-Glu-Phe, was fused to the carboxyl terminus of the α subunit, allowing affinity purification of the heterodimer from *E. coli* extracts, similar to a GGTase-I expression system (22, 23). As in the GGTase-I expression construct, the first 13-aa codons of the α subunit were changed to improve translation and maintain the natural amino acid sequence. FTase was purified by using the same method as described previously for GGTase-I (23), with the following modifications. The YL1/2 antibody CNBr Sepharose fast flow column (Amersham Pharmacia) was scaled up to 200 ml and run without detergent. Both the elution buffer and lysis buffer contained the protease inhibitors benzamide at 10 μg/ml, and aprotinin, leupeptin, and pepstatin at 5 μg/ml each. Pooled fractions were then loaded onto a Mono Q 16/10 column (Amersham Pharmacia) and eluted by a gradient of 0–300 mM NaCl in Mono Q buffer B (1 mM DTT/50 mM Tris·HCl, pH 7.7). The peak FTase fractions were pooled and then combined with an equal volume of 2 M NH_4SO_4 in Phenyl buffer B (100 mM Tris·HCl, pH 7.7/10 mM DTT/5 μM $ZnCl_2$), loaded onto a Phenyl Superose 10/10 column (Pharmacia) and eluted from a 1–0 M NH_4SO_4 gradient in Phenyl buffer B. Peak fractions were pooled, desalted, and concentrated to 10 mg/ml in 20 mM Tris·HCl (pH 7.7) containing 20 mM KCl, 10 μM ZnCl, and 1 mM DTT.

Full-length recombinant rat FTase was expressed by using Sf9 cells, purified as described (24, 25), and concentrated to 16 mg/ml in 20 mM Tris·HCl (pH 7.7) containing 20 mM KCl, 10 μM ZnCl, and 1 mM DTT.

Crystallization. The human FTase·FPP·L-739,750 complex was prepared before crystallization by incubation of human FTase with FPP (20 mM stock FPP solution in 20 mM Tris·HCl, pH 7.7) for 3 h on ice, followed by incubation with L-739,750 (50 mM stock solution in DMSO and 50 mM DTT) for 2 h on ice to yield a 1:3:3 molar ratio (FTase:FPP:L-739,750). The rat FTase·FPP-analog·TKCVFM complex was prepared before crystallization in an analogous manner by first incubating with the FPP analog [20 mM stock solution in 20 mM Tris·HCl, pH 7.7; Fig. 1; FPT Inhibitor II, Calbiochem (26)] for 3 h on ice and then with the TKCVFM peptide (20 mM stock solution in 50 mM DTT; Genosys, The Woodlands, TX) for 2 h on ice to yield a final molar ratio for FTase:FPP analog:TKCVFM of 1:3:3. Crystals of these complexes were grown at 17°C by the method of hanging drop vapor diffusion from drops containing 2 μl of protein solution and 2 μl of reservoir solution [14% (wt/vol) PEG-8000, 200–600 mM ammonium acetate-acetic acid (pH 5.7), and 20 mM DTT].

The rat FTase·FPP·CVFM complex was obtained by soaking a co-crystal of farnesylated-KKKSKTKCVIM product bound to FTase (S.B.L. and L.S.B., unpublished results), in stabilization solution [17% (wt/vol) PEG-8000, 200–600 mM ammonium acetate-acetic acid (pH 5.7), 20 mM KCl, 20 mM Tris·HCl (pH 7.7), and 10 mM DTT] supplemented with 50 μM FPP and 200 μM CVFM peptide (50 mM stock solution in DMSO with 50 mM DTT, gift from Patrick Casey, Duke University, Durham, NC) for a period of 4 days at 17°C. Previous studies have demonstrated that inhibitor compounds soaked into preformed FTase crystals replace the cocrystallized ligands (27). This method is particularly effective because the active site cavity is accessible via the solvent channels that run along the crystallographic six-fold axis.

Crystals were transferred stepwise into cryoprotectant solutions [stabilization solution with 43% (wt/vol) PEG-8000 and 20% (wt/vol) sucrose] containing additional peptide/peptidomimetic and FPP/FPP analog molecules at 20 μM concentrations and flash-cooled.

Crystallographic Data Collection, Structure Determination, and Refinement. Diffraction data were measured at 98 K with an R-axis IV image plate system (Molecular Structure, The Woodlands, TX) mounted on a Rigaku (Tokyo) RU-200 rotating anode generator with double mirror optics (Molecular Structure). DENZO and SCALEPACK were used for data reduction and scaling (28).

All of the crystals belong to the space group $P6_1$ and contain one molecule of FTase per asymmetric unit. Initial phases for the human FTase complex were obtained by molecular replacement in X-PLOR (29) by using the 2.0-Å crystal structure of rat FTase with bound FPP analog and KKKSKTKCVIM peptide as a

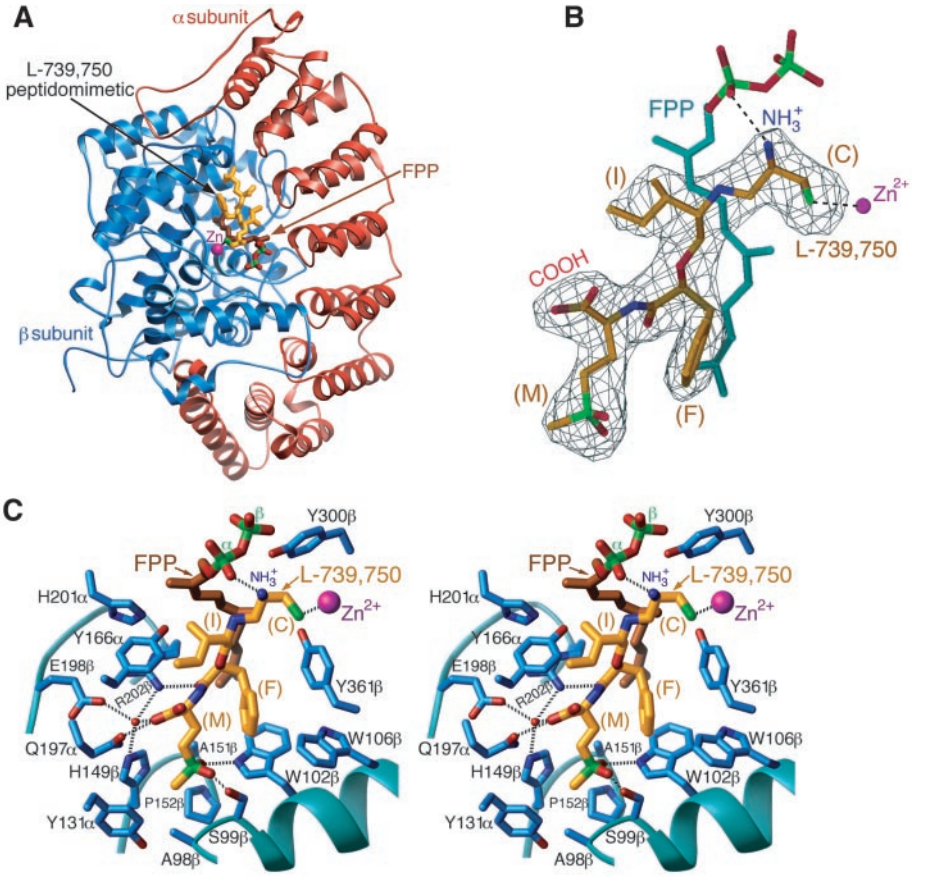

Fig. 2. Structure of human FTase in complex with the CIFM-derived L-739,750 peptidomimetic and FPP substrate. (*A*) Overall structure. (*B*) 6σ F_O-F_C omit electron density for L-739,750. The FPP substrate and zinc ion are included for reference. (*C*) Residues forming van der Waals interactions with L-739,750, shown in stereo. The N terminus of the peptidomimetic forms an ion pair with an α-phosphate oxygen of the FPP substrate.

search model (PDB I.D. code 1D8D; ref. 18). The resulting initial *R* factor was 33%.

The residues that differ between rat and human FTase were consistent with F_O-F_C electron density and were changed to their human counterparts in the model. Difference electron density in the active site of human FTase clearly indicated the presence of well ordered FPP and L-739,750 molecules. The refined model of human FTase contains α subunit residues 55–367 and β subunit residues 17–423, which have continuous, well-defined electron density. As in all structures of FTase determined to date, the proline-rich region of 54 aa at the N terminus of the α subunit is disordered.

Initial phases for the two structures with rat FTase were determined by molecular replacement. There is continuous well-defined electron density for all of the ligand molecules in each of the structures (Fig. 2*B*, Table 1).

Phase calculation and model refinement were done in X-PLOR (29) with a bulk solvent correction (30).

Farnesylation Assays. FTase-mediated transfer of [^{3}H]farnesyl from [^{3}H]FPP to the peptides TKCVIM, TKCVFM, CIIS, and CVFM and L-739,750 was assayed by using TLC (8).

Results and Discussion

Structures of ternary complexes of human FTase with the non-substrate peptidomimetic inhibitor L-739,750 and FPP substrate, rat FTase with the non-substrate inhibitor tetrapeptide CVFM and FPP substrate, and with hexapeptide TKCVFM substrate and a nonreactive FPP analog were determined by x-ray crystallographic methods (Table 1; Fig. 1). In addition, the previously determined complex of rat FTase with TKCVIM is used for structural comparisons (18). Addition of two amino acids at the N terminus in the TKCVFM hexapeptide, converts the CVFM non-substrate inhibitory peptide into an active substrate[§] (9). L-739,750 is a peptidomimetic based on the non-substrate tetrapeptide inhibitor CIFM, but in which the two N-terminal peptide bonds have been replaced with amine or ether linkages (15). These changes introduce extra rotational degrees of freedom in the peptidomimetic compared with a tetrapeptide (Fig. 1). L-739,750 was designed before any structural information about FTase was available and consequently was developed by using well-established empirical approaches of medicinal chemistry.

Rat FTase was used to determine two of the three complexes reported in this study, because rat FTase crystallized more readily and reproducibly than human FTase. Comparison of rat and human structures is valid because the structural differences are limited to regions of crystal contact, and there is complete sequence and structural conservation in the active sites (see below).

Structure of Human FTase. The structure of human FTase is essentially identical to that of the previously reported rat enzyme (24). Structural differences are largely accounted for by replacing the amino acid side chains in the rat structure with

[§]Farnesylation of the peptides TKCVIM, TKCVFM, and CIIS has been demonstrated in this study; FTase did not farnesylate the tetrapeptide CVFM or L-739,750 (data not shown).

Table 1. Data collection and refinement statistics

	Human FTase·FPP·L-739,750	Rat FTase·FPP·CVFM	Rat FTase·FPP analog·TKCVFM
Data collection ($I \geq -3\sigma_I$)			
Resolution, Å	35.0–2.3	50.0–2.0	50.0–2.2
Outer shell, Å	2.40–2.30	2.07–2.00	2.30–2.20
No. reflections			
Unique	52,774	78,430	58,679
Total	294,786	277,944	207,941
Mean I/σ_I*	21.3 (1.9)	26.4 (2.5)	15.0 (2.5)
Completeness, %	99.7	100	99.7
R_{sym}, %*†	7.8 (41.6)	5.4 (39.7)	8.8 (47.0)
Cell, Å, a = b, c	178.5, 64.8	171.2, 69.3	170.9, 69.4
Refinement ($F \geq 2\sigma_F$)			
Completeness, %*	89.0 (69.5)	92.1 (77.1)	89.7 (76.8)
R factor, %*†	17.9 (25.0)	16.7 (24.5)	16.0 (23.7)
R_{free}, %*†	20.9 (24.4)	20.6 (27.6)	20.2 (25.5)
No. non-h atoms	6,321	6,445	6,467
No. solvent	334	430	435
rms			
Bond lengths, Å	0.008	0.007	0.007
Bond angles, °	1.3	1.4	1.4
B-factors, Å^2			
Average	42.1	35.4	34.5
CaaX	37.6	39.1	43.2
FPP substrate or analog	30.8	21.7	22.1
Ramachandran plot			
Most favored, %	91.3	92.0	92.1
Disallowed, %	0	0	0

*Values in parentheses correspond to those in the outer resolution shell.
†$R_{sym} = (\Sigma|(I - \langle I \rangle)|)/(\Sigma I)$, where $\langle I \rangle$ is the average intensity of multiple measurements. R factor and $R_{free} = (\Sigma|F_{obs} - F_{calc}|)/(\Sigma|F_{obs}|)$. R_{free} was calculated using the same ≈5% of structure factors from each data set that were held aside during refinement.

those corresponding to the human sequence. The only significant differences between rat and human FTase structures occur at inter-protein contact points in the crystal lattice, which is consistent with the differences in crystallization properties of these two enzymes. Three regions of crystal contact involving α subunit residues 55–79, and β subunit residues 17–22 and 60–72 have rms deviations of 1.5 Å, 10.1 Å, and 5.2 Å with the rat enzyme (PDB I.D. code 1D8D), respectively. Outside of these regions, the rat and human structures superimpose with an rms deviation of 0.4 Å. The structure of human FTase with bound L-739,750 peptidomimetic is shown in Fig. 2*A*.

Of the 44-aa differences between rat and human FTase, 25 are in the regions of subunit termini that are disordered in both crystals and therefore could not be visualized. All of the remaining 19 differences lie outside of the active site, many occurring on loops that connect pairs of helices in the α subunit. Furthermore, all of the residues that interact with isoprenoid molecules, peptide substrates, and inhibitors in the structures of FTase complexes are conserved between these species and are in nearly identical conformations (17, 18, 27, 31). This structural and sequence conservation indicates that either enzyme serves well for development and optimization of FTase inhibitors.

L-739,750 Peptidomimetic Conformation. The peptidomimetic inhibitor L-739,750 (Fig. 1) (13, 16), which is intended to mimic the tetrapeptide CIFM, adopts an extended conformation in the active site of FTase rather than the β-turn observed in NMR studies (16). Coordination of the N-terminal cysteine thiol(ate) to the catalytic zinc ion is preserved in this peptidomimetic complex (Fig. 2*C*). The carboxyl terminus of the peptidomimetic makes the same hydrogen bonding interactions with FTase as peptide substrates (17, 18). FPP adopts the same conformation as seen in all other FTase complexes with bound FPP substrate (17, 27, 31) and shares the same conformation as FPP analogs, except for differences among these analogs within the first isoprene unit (17, 18). The FPP interacts extensively with L-739,750 (Fig. 2). The structure of the part of the peptidomimetic that corresponds to the a_2X portion of the Ca_1a_2X motif is nearly identical to that observed in substrates (0.7 Å rms deviation with the K-Ras4B-derived peptide substrate TKCVIM for corresponding atoms; ref. 18). This region forms the same interactions with FTase as observed in cognate peptide substrates (refs. 17 and 18). The oxygen atoms of the sulfone substitution in the methionine side chain of L-739,750 form hydrogen bonds with Ser-99β and Trp-102β (Fig. 2*C*). The phenylalanine residue of L-739,750 has extensive van der Waals interactions with Tyr-361β, Trp-102β, and Trp-106β, as well as the isoprenoid of FPP.

The most striking conformational difference compared with the peptide substrate is within the N-terminal Ca_1 portion of Ca_1a_2X peptidomimetic. This portion of the peptidomimetic has a 2.2 Å rms deviation with the TKCVIM peptide substrate for analogous atoms, by virtue of a change in the backbone angles between the a_2 and a_1 positions. As a result, the positively charged N terminus of L-739,750 forms an ion pair with an α-phosphate oxygen of the FPP substrate (Fig. 3*A*), an interaction that is not present in longer peptide substrates or proteins for the simple reason that their N termini are further away (Fig. 3*B*). The thiol(ate) of the N-terminal cysteine is located in a position identical to that observed in substrates, thereby retaining the bond to the zinc, but the cysteine adopts a different rotamer to maintain this bond. In the non-substrate conformation, the N-terminal moiety is juxtaposed between the zinc and FPP, changing the geometry of the thiol C_β-S_γ bond, which now points away from the FPP substrate. Consequently, the interaction between the reactive groups of the two substrates has been altered radically.

Non-Substrate Tetrapeptide CVFM Conformation. The non-substrate CVFM tetrapeptide adopts the same conformation as L-739,750, with an rms deviation of 0.6 Å for analogous atoms (Fig. 3*A*). This result indicates that L-739,750 truly mimics the tetrapeptide despite the increased torsional flexibility of L-739,750. Furthermore, the CVFM peptide also forms an ion pair between its N terminus and the FPP α-phosphate. As is the case for L-739,750, the structure of the part of the CVFM tetrapeptide corresponding to the a_2X portion of the Ca_1a_2X motif is nearly identical to that observed in the K-Ras4B-derived peptide substrate TKCVIM (0.28 Å rms deviation for corresponding atoms). Although the backbone conformation of the X residue is the same between these two peptides, there is a difference between the TKCVIM substrate and CVFM non-substrate peptides in the ϕ/ψ backbone Ramachandran angles of the a_2 residue (Table 2). This difference is to be an important factor determining the farnesylation of CaaX tetrapeptides (see below).

Hexapeptide Substrate TKCVFM Conformation. The TKCVFM peptide adopts the same conformation as the K-Ras4B-derived peptide substrate TKCVIM in an analogous complex (ref. 18; Fig. 3*B*), consistent with the observation that it is also a substrate (9, 32). The two hexapeptides have an rms deviation of 0.38 Å for superimposable atoms. The valine residue at the a_1 position has a different side chain rotamer conformation, which is correlated with a concerted change in the conformation of the first isoprene unit of the FPP analog, thereby accommodating steric packing interactions between the FPP

BIOCHEMISTRY

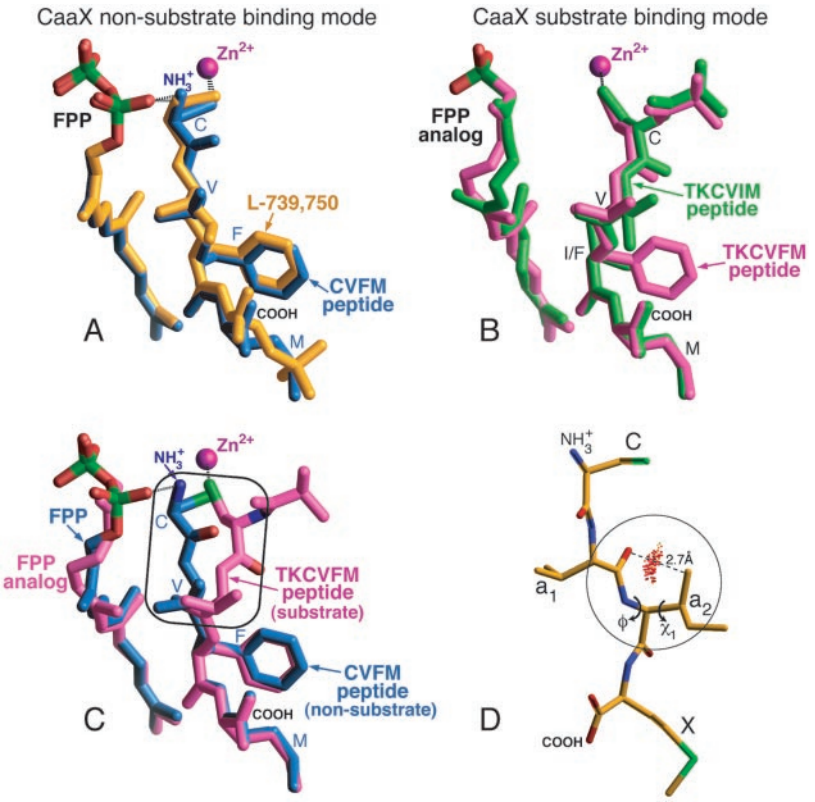

Fig. 3. Comparison of CaaX non-substrate and substrate conformations. The superpositions are based on all FTase C_α atoms. The same orientation is shown in each panel. (*A*) CaaX tetrapeptide non-substrate inhibitor binding conformation. L-739,750 peptidomimetic and CVFM tetrapeptide shown with the FPP molecules observed in these two complexes colored yellow (with peptidomimetic) and blue (with CVFM tetrapeptide). Note that the valine to isoleucine substitution at the a_1 position of the Ca_1a_2X motif does not affect the conformation of these two inhibitors, consistent with the orientation of these residues toward bulk solvent. (*B*) Peptide substrate binding conformation. TKCVFM and the K-Ras4B peptide TKCVIM (18) are both substrates and adopt the same backbone conformation. The N-terminal residue and the lysine side chain of each of these peptides are omitted from the figure for clarity. Also shown are the FPP analogs (Fig. 1), which are colored according to their observed conformations with these peptides. (*C*) Comparison of the hexapeptide substrate TKCVFM and the non-substrate tetrapeptide inhibitor CVFM. A boxed region highlights the differences between the substrate and non-substrate conformations. (*D*) Energetically unfavorable steric contact (red spikes) between the $C_{\gamma 2}$ methyl group of the isoleucine residue in the a_2 position and the carbonyl oxygen of the a_1 residue when the phenylalanine residue of the CVFM tetrapeptide is replaced with isoleucine. Consequently, a tetrapeptide with a β-branched residue (isoleucine or valine) in the a_2 position cannot adopt the non-substrate binding mode observed for CVFM. These steric contacts were displayed by using the programs PROBE and REDUCE (34) in conjunction with the program O (35).

analog and amino acid side chain (Fig. 3*B*, Table 2). As with the L-739,750 peptidomimetic, the only significant deviations between CVFM and TKCVFM are at the N terminus of the tetrapeptide (Fig. 3*C*). This result strongly suggests that N-terminal interaction with the FPP α-phosphate is the dominant determinant of CaaX tetrapeptide farnesylation, consistent with biochemical observations (9).

Structural Basis of CaaX Peptidomimetic Inhibition. We propose that certain tetrapeptides are not able to act as substrates because they bind in a nonproductive conformation that is stabilized by an ion pair formed between their N terminus and the FPP α-phosphate. This conformation radically alters the geometry of the cysteine, despite the maintenance of the Zn-thiol(ate) bond, and interferes with the formation of the transition state required for catalysis.

The sequence determinants that distinguish tetrapeptide substrates from non-substrates are subtle, and appear to involve *destabilizing* interactions that *prevent* peptides from becoming non-substrates, rather than *stabilizing* interactions that *promote* formation of a non-productive complex. The critical change in backbone geometry that determines whether a tetrapeptide adopts a substrate or non-substrate conformation occurs in the backbone geometry between residues in the a_1 and a_2 positions. The side chains in the a_2 position adopt essentially the same conformation in all peptides, thereby filling a complementary hydrophobic pocket in the protein. This side-conformation places steric constraints on the ϕ backbone angle (defined as the torsion involving atoms C_{i-1}, N_i, $^{\alpha}C_i$, and C_i) between the a_1 and a_2 residues. β-branched amino acids (isoleucine and valine) in the a_2 position form an unfavorable steric interaction between their $C_{\gamma 2}$ methyl group and the carbonyl oxygen of the a_1 residue in the non-substrate backbone conformation adopted by the CVFM peptide (Fig. 3*D*). Conformational mapping calculations indicate that tetrapeptides with isoleucine or valine residues in the a_2 position cannot adopt the non-substrate conformation, whereas no unfavorable interactions are formed in the substrate conformation (Fig. 4). By contrast, these calculations show that peptides with a phenylalanine, alanine, or leucine in this position can adopt either conformation without forming unfavorable interactions.

Tetrapeptides with β-branched amino acids in the a_2 position (such as isoleucine in CVIM) therefore are obligate substrates, because on steric grounds they cannot adopt the

Table 2. Dihedral angles of the Ca_1a_2X residues*

	CVFM			TKCVIM			TKCVFM		
	ϕ	ψ	χ_1	ϕ	ψ	χ_1	ϕ	ψ	χ_1
C	NA†	167	53	−105	139	−89	−92	129	−81
a_1	−150	178	−68	−117	132	177	−90	142	−59
a_2	−154	−25	70	−126	7	65	−139	−9	58
X	−165	NA†	82	−171	NA†	78	−166	NA†	79

*ϕ, angle of rotation around the N–C_α bond; ψ, angle of rotation around the C_α–C′ bond; χ_1, angle of rotation around the C_α–C_β bond (units are degrees; angles defined using the standard conventions).
†NA, not applicable.

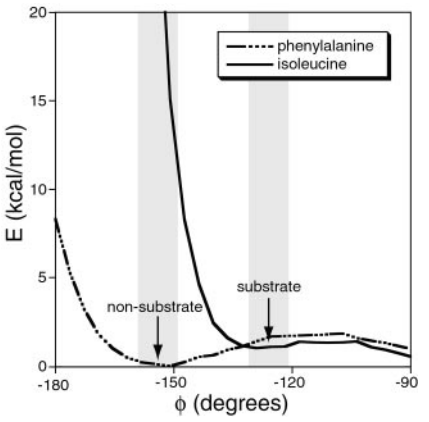

Fig. 4. Conformational maps comparing placement of isoleucine (solid line) and phenylalanine (dashed line) in the a_2 position of a tetrapeptide that adopts a non-substrate conformation. The coordinates of the CVFM peptide complex were used as a representative non-substrate conformation. Only the a_1a_2 dipeptide was considered in the calculation. Shown are the contributions to the van der Waals interactions as the ϕ dihedral angle between the a_1 and a_2 positions is varied. For each sampled value of this angle, the χ_1 dihedral angles of the side chains in the a_1 (valine) and a_2 (isoleucine, valine, phenylalanine, leucine, or alanine) positions were allowed to vary within $\pm 30°$ of the values observed in the crystal structure, and the minimum local energy was recorded. In the a_2 position, valine resulted in a curve similar to isoleucine, whereas leucine and alanine yielded curves similar to phenylalanine (not shown). The shaded areas indicate the two regions in the vicinity of the non-substrate ($\phi = -154°$, arrow) and substrate ($\phi = -126°$, arrow) conformations, respectively (the conformational map outside these regions is not relevant, because the tetrapeptide is not observed to adopt such conformations in the FTase active site). Conformational maps were generated by using the DEZYMER program (36, 37).

non-substrate conformation corresponding to the CVFM tetrapeptide. Amino acids that are not branched at this position can adopt either the substrate or non-substrate conformation, the latter being preferentially stabilized by formation of the N-terminal ion pair with the FPP α-phosphate. In such peptides, an equilibrium between the substrate and non-substrate conformations must therefore exist. We therefore predict that, of the CaaX cognate tetrapeptides, only peptides with isoleucine or valine in the a_2 position are substrates, whereas peptides with other aliphatic amino acids that are not β-branched are poor or non-substrates (provided that the N terminus is not blocked). This interpretation is also consistent with the observation that CaaX tetrapeptide mimetics that have a β-branched side chain in the a_2 position are non-substrate inhibitors if the two N-terminal peptide bonds are reduced, eliminating the carbonyl oxygen of the a_1 residue [e.g., the non-substrate peptidomimetic L-731,735 derived from the tetrapeptide substrate CIIS (11, 33)]. A detailed understanding of the sequence determinants of steric interactions will facilitate further design of more effective FTase inhibitors.

We thank Charles A. Omer for design of the human FTase expression vector; Jane S. DeSolms for the L-739,750 peptidomimetic inhibitor; Jackson B. Gibbs, Patrick J. Casey, and Jane S. Richardson for helpful discussions; Kendra E. Hightower for help with the farnesylation assay; and Joel Tuttle for assistance with crystallization. The work was supported by a Merck Research Study Agreement and National Institutes of Health Grant GM52382 (to L.S.B.) and by an American Heart predoctoral fellowship to (S.B.L.).

1. Casey, P. J. (1995) *Science* **268,** 221–225.
2. Zhang, F. L. & Casey, P. J. (1996) *Annu. Rev. Biochem.* **65,** 241–269.
3. Ashar, H. R., James, L., Gray, K., Carr, D., Black, S., Armstrong, L., Bishop, W. R. & Kirschmeier, P. (2000) *J. Biol. Chem.* **275,** 30451–30457.
4. Schafer, W. R., Kim, R., Sterne, R., Thorner, J., Kim, S.-H. & Rine, J. (1989) *Science* **245,** 379–385.
5. Casey, P. J., Solski, P. A., Der, C. J. & Buss, J. E. (1989) *Proc. Natl. Acad. Sci. USA* **86,** 8323–8327.
6. Hancock, J. F., Magee, A. I., Childs, J. E. & Marshall, C. J. (1989) *Cell* **57,** 1167–1177.
7. Reiss, Y., Goldstein, J. L., Seabra, M. C., Casey, P. J. & Brown, M. S. (1990) *Cell* **62,** 81–88.
8. Goldstein, J. L., Brown, M. S., Stradley, S. J., Reiss, Y. & Geirasch, L. M. (1991) *J. Biol. Chem.* **266,** 15575–15578.
9. Brown, M. S., Goldstein, J. L., Paris, K. J., Burnier, J. P. & Marsters, J. C. (1992) *Proc. Natl. Acad. Sci. USA* **89,** 8313–8316.
10. Moores, S. L., Schaber, M. D., Mosser, S. D., Rands, E., O'Hara, M. B., Garsky, V. M., Marshall, M. S., Pompliano, D. L. & Gibbs, J. B. (1991) *J. Biol. Chem.* **266,** 14603–14610.
11. Williams, T. M. & Dinsmore, C. J. (1999) *Adv. Med. Chem.* **4,** 273–314.
12. Sepp-Lorenzino, L., Ma, Z., Rands, E., Kohl, N. E., Gibbs, J. B., Oliff, A. & Rosen, N. (1995) *Cancer Res.* **55,** 5302–5309.
13. Kohl, N. E., Omer, C. A., Conner, M. W., Anthony, N. J., Davide, J. P., deSolms, S. J., Giuliani, E. A., Gomez, R. P., Graham, S. L., Hamilton, K., *et al*. (1995) *Nat. Med.* **1,** 792–797.
14. Johnston, S. R. D. (2001) *Lancet Oncol.***2,** 18–26.
15. Kohl, N. E., Wilson, F. R., Mosser, S. D., Giuliani, E., deSolms, S. J., Conner, M. W., Anthony, N. J., Holtz, W. J., Gomez, R. P., Lee, T. J., *et al*. (1994) *Proc. Natl. Acad. Sci. USA* **91,** 9141–9145.
16. Koblan, K. S., Culberson, J. C., deSolms, S. J., Giuliani, E. A., Mosser, S. D., Omer, C. A., Pitzenberger, S. M. & Bogusky, M. J. (1995) *Protein Sci.* **4,** 681–688.
17. Strickland, C. L., Windsor, W. T., Syto, R., Wang, L., Bond, R., Wu, Z., Schwartz, J., Le, H. V., Beese, L. S. & Weber, P. C. (1998) *Biochemistry* **37,** 16601–16611.
18. Long, S. B., Casey, P. J. & Beese, L. S. (2000) *Structure Fold. Des.* **8,** 209–222.
19. Huang, C.-C., Casey, P. J. & Fierke, C. A. (1997) *J. Biol. Chem.* **272,** 20–23.
20. Hightower, K. E., Huang, C.-C., Casey, P. J. & Fierke, C. A. (1998) *Biochemistry* **37,** 15555–15562.
21. Eisenberg, S. P., Evans, R. J., Arend, W. P., Verderber, E., Brewer, M. T., Hannum, C. H. & Thompson, R. C. (1990) *Nature (London)* **343,** 341–346.
22. Omer, C. A., Kral, A. M., Diehl, R. E., Prendergast, G. C., Powers, S., Allen, C. M., Gibbs, J. B. & Kohl, N. E. (1993) *Biochemistry* **32,** 5167–5176.
23. Omer, C. A., Diehl, R. E. & Kral, A. M. (1995) *Methods Enzymol.* **250,** 3–12.
24. Park, H.-W., Boduluri, S. R., Moomaw, J. F., Casey, P. J. & Beese, L. S. (1997) *Science* **275,** 1800–1804.
25. Chen, W.-J., Moomaw, J. F., Overton, L., Kost, T. A. & Casey, P. J. (1993) *J. Biol. Chem.* **268,** 9675–9680.
26. Manne, V., Ricca, C. S., Brown, J. G., Tuomari, A. V., Yan, N., Patel, D., Schmidt, R., Lynch, M. J., Ciosek, C. P., Jr., Carboni, J. M., *et al*. (1995) *Drug Dev. Res.* **34,** 121–137.
27. Strickland, C. L., Weber, P. C., Windsor, W. T., Wu, Z., Le, H. V., Albanese, M. M., Alvarez, C. S., Cesarz, D., del Rosario, J., Deskus, J., *et al*. (1999) *J. Med. Chem.* **42,** 2125–2135.
28. Otwinowski, Z. & Minor, W. (1997) *Methods Enzymol.* **276A,** 307–326.
29. Brünger, A. T. (1992) X-PLOR, A System for X-Ray Crystallography and NMR (Yale Univ. Press, New Haven, CT), Version 3.1.
30. Brünger, A. T. & Jiang, J. S. (1994) *J. Mol. Biol.* **243,** 100–115.
31. Long, S., Casey, P. J. & Beese, L. S. (1998) *Biochemistry* **37,** 9612–9618.
32. Stradley, S. J., Rizo, J. & Gierasch, L. M. (1993) *Biochemistry* **32,** 12586–12590.
33. Kohl, N. E., Mosser, S. D., deSolms, S. J., Giuliani, E. A., Pompliano, D. L., Graham, S. L., Smith, R. L., Scolnick, E. M., Oliff, A. & Gibbs, J. B. (1993) *Science* **260,** 1934–1942.
34. Word, J. M., Lovell, S. C., LaBean, T. H., Taylor, H. C., Zalis, M. E., Presley, B. K., Richardson, J. S. & Richardson, D. C. (1999) *J. Mol. Biol.* **285,** 1711–1733.
35. Jones, T. A. & Kjeldgaard, M. (1993) O**,** The Manual (Uppsala University, Uppsala), Version 5.9.
36. Hellinga, H. W. & Richards, F. M. (1991) *J. Mol. Biol.* **222,** 763–785.
37. Looger, L. L. & Hellinga, H. W. (2001) *J. Mol. Biol.* **307,** 429–445.